Decoupling-free NMR quantum computer on a quantum spin chain

Atsushi Goto,* Tadashi Shimizu, Kenjiro Hashi, Hideaki Kitazawa, and Shinobu Ohki
Nanomaterials Laboratory, National Institute for Materials Science, Sakura, Tsukuba 305-0003, Japan and CREST, Japan Science and Technology Corporation, Kawaguchi, Saitama 332-0012, Japan
(Received 21 May 2002; published 28 February 2003)

We propose a decoupling-free nuclear-spin quantum computer installed on a quantum electron spin chain with a singlet ground state and a finite spin gap. Qubits are $I=1/2$ nuclear spins implanted periodically along the quantum spin chain. A magnetic field gradient is applied parallel to the chain, which allows individual access to each qubit. A single-qubit operation (rotation gate) is realized with the rf field tuned to the nuclear Larmor frequency at the qubit of interest, while a two-qubit operation (controlled-NOT gate) is achieved using the Suhl-Nakamura interaction through a packet of triplet magnons, which are excited by a microwave tuned to the spin gap energy (*SN* gate). The interaction can be switched off by turning off the microwave, and a decoupling-free quantum computer is realized. The initialization is achieved with an optical pumping qubit initializer, which has a multilayered structure of the quantum spin chain and a semiconductor. Spin polarizations created by the optical pumping in the semiconducting layers are transferred to the spin chain layers through a cross polarization and a spin diffusion. The scheme allows us to separate the initialization process from the computation, enabling us to optimize the latter independently of the former.

DOI: 10.1103/PhysRevA.67.022312 PACS number(s): 03.67.Lx, 76.60.−k, 75.45.+j

I. INTRODUCTION

A quantum computer (QC) is a Turing machine that performs information processing based on the principles of quantum mechanics [1]. Its features such as superposition and entanglement of quantum states enable parallel computation for all the possible states simultaneously, which allows us to deal with the problems that are formidable for classical computers. Recent progress in the quantum algorithm [1–3] has spurred the implementation of the QC in actual physical systems. Among other systems proposed so far, a nuclear-spin system is one of the most promising candidates, because of the good isolation from the environment and good controllability with the well-established technique of nuclear magnetic resonance (NMR) [4]. The first NMR QC was implemented by molecules in solutions [5,6], which shows great promise for NMR QCs.

The current most crucial concern in the NMR-QCs is scalability; although a seven-qubit QC has been realized with a solution [7], it seems rather difficult for the number of qubits (q) to be far beyond ten in this scheme because of the following reasons: (1) The number of available nuclei in one molecule is limited. (2) The number of available molecules in the pseudopure state [8–10] is proportional to $(\hbar\omega_n/2k_BT)q/2^q$, so that the signal intensity from these molecules becomes smaller with increasing q, and is eventually smeared out in thermal noises. The QC needs at least 100 qubits to surpass its classical analog [2]; so it is crucial to provide an alternative scheme that enables a systematic increase of q. One promising scheme is to utilize a crystal instead of a solution [11], which lifts away the limitation on the number of available nuclei. A magnetic-field gradient applied to the crystal produces a distribution of the nuclear Larmor frequency ω_n, which provides a means to distinguish qubits. A single-qubit operation (rotation gate) is achieved with the rf field with ω_n at each qubit, while a two-qubit operation (controlled-NOT gate) is performed using a nuclear dipole (direct) coupling between adjacent qubits one lattice constant apart with the pulse sequence shown in Fig. 1(a).

We find, however, that the nuclear dipole coupling is inappropriate for this scheme because of the following reasons. One is that it requires a huge magnetic-field gradient ($\delta H/\delta x$) to distinguish each individual qubit: actually, $\delta H/\delta x = 1\ \mathrm{T}/\mu\mathrm{m}$ is still marginal for the interqubit distance δx of one lattice constant [12]. Since the difference in ω_n between adjacent qubits, $\delta\omega_n$, is proportional to $\delta x\,\delta H/\delta x$, one could increase δx to reduce $\delta H/\delta x$, but this requires a long-range interqubit coupling. The dipolar coupling is unfortunate because it can reach at most a few lattice spacings [13]. The other is that it requires continuous applications of decoupling sequences to remove unwanted couplings, because it is always present whenever two qubits are close to each other. As q is increased, the number of decoupling sequences increases as q^2. Though this dependence is still a polynomial function of q, it actually consumes a huge amount of time and reduces the effective number of steps possible within the coherence time.

These facts motivate us to seek a long-range indirect coupling mediated by electrons. They include J couplings in covalent bondings, Ruderman-Kiftel-Kasuya-Yosida interactions in metals [14], and Suhl-Nakamura (SN) interactions in magnets [15,16]. Among them, the SN interaction has the characteristics preferable for the present purpose, such as the long-range nature and the externally controllable coupling strength. In this paper, we present the scheme of the NMR QC with the interqubit coupling mediated by the SN interaction, which is specifically called the SN gate [17]. The advantages of the scheme are that the pulse sequence can be simpler due to the absence of unnecessary couplings, and that δx can be set larger, which relieves the constraints on

*Electronic address: GOTO.Atsushi@nims.go.jp

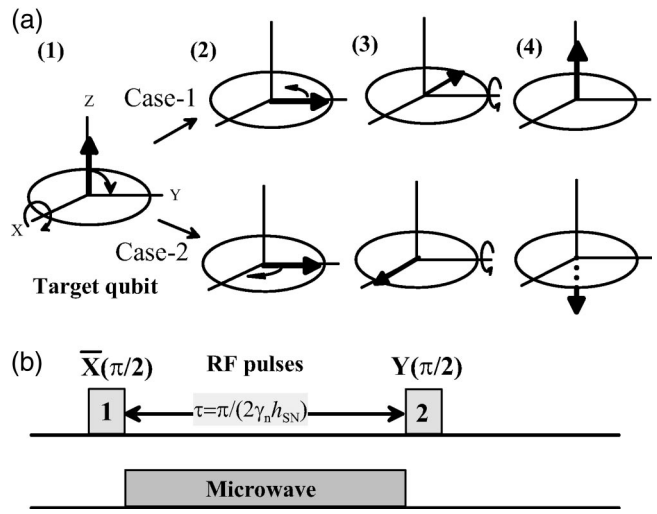

FIG. 1. (a) Schematic illustration of the controlled-NOT gate in the rotating frame of the target (T) qubit. Upper and lower figures correspond to the cases for the control C qubit being $\uparrow$ (case 1) and $\downarrow$ (case 2), respectively. (1) The T-qubit spin is in the up state. The spin is rotated by a $\overline{X}(\pi/2)$ pulse around the negative X axis. (2) The spin starts to turn in the XY plane due to the additional field caused by the C qubit. (3) The spin turns by $\pm 90°$ to the positive or negative X direction in the XY plane. (4) The spin is rotated again by a $Y(\pi/2)$ pulse around the positive Y axis. The direction of the spin with respect to Z is hereby controlled according to the spin state of the C qubit. (b) Corresponding sequences for the rf pulses and the microwave irradiation in the SN-gate operation.

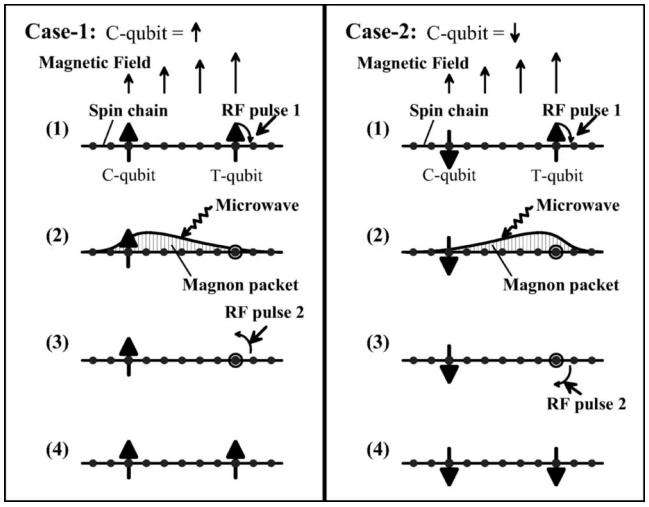

FIG. 2. Schematic illustration of the SN-gate (controlled-NOT gate) operation under the magnetic-field gradient shown at the top. Horizontal lines are quantum spin chains, and dots and arrows on the lines are zero-spin and half-spin nuclei (i.e., qubits), respectively. The symbols $\odot$ represent the qubit in the XY plane. Cases 1 and 2 correspond to the C qubit being $\uparrow$ and $\downarrow$, respectively. See the corresponding figures in Fig. 1. (1) A rf pulse 1 ($\pi/2$) is applied to the T qubit. (2) A microwave is turned on, which excites a magnon packet between the qubits (hatched part). The T qubit is rotated in the XY plane due to the additional field (h_{SN}) caused by the magnon packet. (3) After the time $\tau=\pi/(2\gamma_n h_{SN})$, the microwave is turned off and a pulse 2 ($\pi/2$) is applied to the T qubit. (4) The T qubit is rotated back to $\uparrow$ (case 1) or forth to $\downarrow$ (case 2). Note that the applied rf and microwave frequency are the same for both cases 1 and 2.

$\delta H/\delta x$. We also present an effective initialization scheme suitable for the present scheme, called the optical pumping qubit initializer, which is an effective nuclear polarizer that makes use of the optical pumping and the polarization transfer methods. It allows us to separate the initialization scheme from the computation, so that the latter can be optimized independently of the former.

II. OUTLINE OF THE SN-GATE

Here, we present the outline of the SN-gate operation. The system configuration and the operation procedure are schematically illustrated in Fig. 2. The system consists of a one-dimensional array of electron spins (quantum spin chain) placed in a magnetic-field gradient produced by a magnet fabricated outside the system [18]. Suppose that the electrons are in the singlet ground state ($|ss_z\rangle=|00\rangle$) with a finite gap to the lowest triplet excitation state ($|1-1\rangle$) due to some quantum effects. Examples include spin ladder, Haldane, dimer and spin-Peierls systems. Also suppose that nuclei ($I=1/2$) serving as qubits are placed periodically, e.g., every ten lattice points ($10a$), each of which has a hyperfine coupling with the electron spins. In the ground state, the qubits are well isolated from the environment because of the absence of unpaired electron spins [Fig. 2,(1)].

Here, the qubits are also isolated from each other due to the absence of interqubit couplings; the nuclear dipole interactions between qubits are negligibly small because of the large spatial separation between qubits. Moreover, the Suhl-Nakamura interaction, which is known to remain finite even in the singlet ground state due to the exchange of virtual magnons [15,16], is also negligible in the present situation because of the following reasons. Its transverse component with a form of $I_i^+ I_j^-$ is absent in the field gradient because of the detuning effect, i.e., a mismatch in the nuclear Zeeman energies prevents the nuclei from exchanging magnons. On the other hand, the longitudinal component ($I_i^z I_j^z$) is ineffective for the pair of qubits $10a$ apart, because the interaction, which is characterized by an antiferromagnetic spin-spin correlation function (see Sec. IV) [19–21], is short-ranged, so that it does not reach more than a few lattice spacings [22].

In order for the system to work as a QC, one has to provide logic gates. A complete QC should be equipped with arbitrary rotation R and controlled-NOT gates [23]. The R gate is realized by the rf pulse with the corresponding nuclear Larmor frequency, while the controlled-NOT gate is realized with an interqubit coupling between the control (C) and target (T) qubits. Since the controlled-NOT gate between any combination of qubits far apart can be realized by a series of gate operations between *adjacent* qubits [24], a coupling between adjacent qubits is the necessary and sufficient condition for the gate. This coupling, however, is needed only between the C and T qubits, and only during the controlled-NOT gate operation. Our strategy to create this local and temporary coupling is to use the electron-spin triplet states excited only between the C and T qubits.

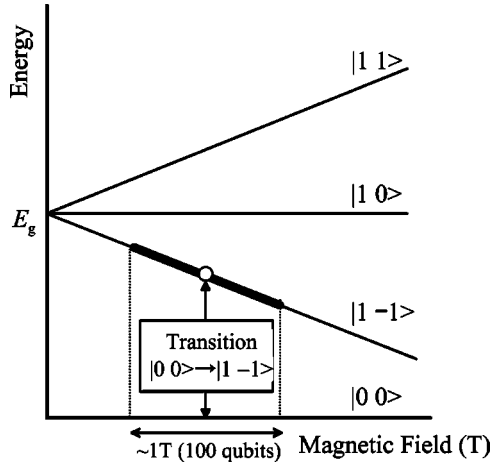

FIG. 3. Energy diagrams for the three triplet branches ($|11\rangle$,$|10\rangle$ and $|1-1\rangle$) of the $k=0$ magnon excitation modes against the singlet state ($|00\rangle$) as a function of the external field. In the field gradient, the horizontal axis also corresponds to the position along the chain. The thick line on the $|1-1\rangle$ branch shows a part of the chain used as a QC, and an open circle is the spot where the transition ($|00\rangle \rightarrow |1-1\rangle$) occurs.

The transition between singlet and triplet states by microwave irradiation is used to create the electron triplet states. Although the transition is primarily forbidden for the usual electric dipolar transition, it often becomes possible in the actual systems because of some higher-order terms in the electron-photon interaction Hamiltonians [25,26]. The position of the excited triplet states along the chain is specified by the microwave frequency, which is uniquely given in the field gradient. The energy diagrams of the $k=0$ magnon excitations in the magnetic field are shown in Fig. 3 [27,25]. In the field gradient, the magnetic field at each part of the chain is unique so that the excitation energy to the lowest triplet state ($|1-1\rangle$) is also uniquely given, which provides a spatial resolution of the excitation. The irradiation of the microwave creates a packet of superpositions of $|00\rangle$ and $|1-1\rangle$ [25], corresponding to the magnon excitations with the wave number $k\sim 0$. The number of the excited triplet states (n) is determined by the balance between the excitation to the $|1-1\rangle$ state and the relaxation (with the lifetime of T_s) to the ground state.

The SN gate is performed with the additional field at the T qubit caused by the SN interaction with the C qubit (h_{SN}). The origin of h_{SN} can be explained intuitively in terms of the *nuclear field*. The nuclear field is a magnetic field produced by a nuclear spin, which is superimposed on the external magnetic field. In the present case, the nuclear field produced by the C qubit distorts the magnetic-field profile along the chain, which is felt by the electrons excited by the microwave. As a result, the distribution of the triplet state density along the chain is distorted depending on the spin state of the C qubit as shown in Fig. 2 (2), so is the spin density at the T qubit. h_{SN} corresponds to the change in the spin density at the T qubit caused by the C qubit. Note that the rf and microwave frequency are determined irrelevantly to the spin states of the C qubit. Beside h_{SN}, the triplet states also make an additional field (H_{tr}) associated with the "shift" at the T qubit, which can be determined as follows; under the microwave irradiation, one observes the shift at the T qubit while saturating the C qubit by applying the corresponding rf field continuously. The saturation of the C qubit results in $h_{\mathrm{SN}}=0$ at the T qubit, so that the observed shift directly corresponds to H_{tr}.

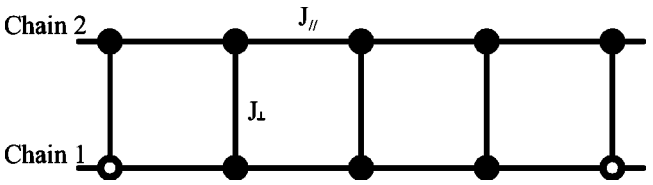

FIG. 4. A spin-ladder configuration. Closed and open circles represent zero- and half-spin (i.e., qubit) nuclei, respectively.

With this local SN interaction, the SN gate (controlled-NOT gate) is achieved as follows (see Figs. 1 and 2).

(1) In the initial state, the T qubit is assumed to be in the up state. The rf pulse 1 [$\overline{X}(\pi/2)$, $\omega=\omega_0\equiv\gamma_n H(T)$, where $H(T)$ is the magnetic field at the T qubit] is applied.

(2) A microwave is applied to the system. The SN interaction is switched on, and the T qubit starts to rotate in the XY plane of the rotating frame with $\omega_1=\gamma_n[H(T)+H_{tr}]$ (Note that ω_1 is different from that before the microwave irradiation, ω_0). The direction of the rotation with respect to the rotating frame depends on the state of the C qubit (up or down).

(3) After the time $\tau=\pi/(2\gamma_n h_{\mathrm{SN}})$, the T qubit reaches either the positive or negative X.

(4) The SN interaction is turned off by shutting off the microwave, and the rf pulse 2 [$\mathrm{Y}(\pi/2), \omega=\omega_0$] is applied, which rotates the T qubit upward or downward according to the C qubit, and the controlled-NOT gate is completed.

III. SINGLET-TRIPLET EXCITATIONS IN THE QUANTUM SPIN CHAIN

One of the key phenomena in the SN-gate operation is the selective excitations of the triplet states shown in Fig. 3 [25]. Let us see the excitations in detail. We consider the spin-ladder case shown in Fig. 4 as an example, and follow the description in Ref. [27]. The effective *spin* is introduced within the subspace consisting of the ground state $|00\rangle$ and the lowest excited state $|1-1\rangle$. This treatment is helpful to visualize the transition as a rotation of the *spin*.

The Hamiltonians that govern the electron system are

$$H=H_0+H_1, \tag{1}$$

$$H_0=J_{\perp}\sum_i \mathbf{s}_{i1}\cdot\mathbf{s}_{i2}+g\mu_B\sum_i \mathbf{H}(x_i)\cdot(\mathbf{s}_{i1}+\mathbf{s}_{i2}), \tag{2}$$

$$H_1=J_{\parallel}\sum_{nn} \mathbf{s}_{i1}\cdot\mathbf{s}_{j1}+J_{\parallel}\sum_{nn} \mathbf{s}_{i2}\cdot\mathbf{s}_{j2}. \tag{3}$$

Here, $J_{\perp}$ and $J_{\parallel}$ are the intrapair (rung) and interpair (leg) exchange interactions, respectively. $\mathbf{H}(x_i)$ is the external field at the ith site and "nn" means the nearest-neighbor

sites. By introducing the operators $\mathbf{S}_i=\mathbf{s}_{i1}+\mathbf{s}_{i2}$ and $\mathbf{T}_i=\mathbf{s}_{i1}-\mathbf{s}_{i2}$, Eqs. (1)–(3) are rewritten as

$$H_0=\frac{1}{2}J_\perp\sum_i \mathbf{S}_i^2+g\mu_B\sum_i \mathbf{H}(x_i)\cdot\mathbf{S}_i, \tag{4}$$

$$H_1=\frac{1}{2}J_\parallel\sum_{nn}(\mathbf{S}_i\cdot\mathbf{S}_j+\mathbf{T}_i\cdot\mathbf{T}_j), \tag{5}$$

where some constant terms have been dropped.

We further rewrite these Hamiltonians in terms of the Pauli spin components in the following manner:

$$\mathbf{S}_i^2=1-\sigma_i^z,\quad S_i^x=S_j^x=0,\quad S_i^z=\frac{1}{2}(\sigma_i^z-1),$$

$$T_i^x=\frac{1}{\sqrt{2}}\sigma_i^x,\quad T_i^y=\frac{1}{\sqrt{2}}\sigma_i^y,\quad T_i^z=0. \tag{6}$$

As a consequence of these transformations, the two states of $|00\rangle$ and $|1-1\rangle$ can be treated as the two spin states represented by the Pauli spin matrices. The total Hamiltonian, Eq. (1), is expressed by these spin matrices as

$$H=\frac{N}{2}\left(J_\perp+\frac{J_\parallel}{4}-g\mu_B\sum_i H(x_i)\right)-\frac{1}{2}\sum_i\left\{J_\perp+\frac{J_\parallel}{4}-g\mu_B H(x_i)\right\}\sigma_{zi}+\frac{J_\parallel}{8}\sum_{nn}\{2(\sigma_i^x\sigma_j^x+\sigma_i^y\sigma_j^y)+\sigma_i^z\sigma_j^z\}. \tag{7}$$

This describes the system of *spins* coupled through anisotropic exchange interactions. The microwave rotates these *spins*, and the small-angle rotations of the *spins* create a packet of triplet states ($k\sim 0$ magnons) like a soliton.

Here, the key issue is the mobility of the packet, because a movable packet could not provide a stable SN coupling. Actually, the packet is localized on the chain due to the magnetic-field gradient; a mismatch in the excitation energies between adjacent regions along the chain prohibits the packet from moving to the lower-field region. On the other hand, the continuum excitations near the one-magnon excitations at $k=0$ is absent, so that it is difficult for the packet to move to the higher-field region [28–32] unless the process of the energy release by phonon emissions is considerable. Consequently, the packet of the triplet states is *confined* in the region where it is excited, and the stable SN interaction is produced only between the C and T qubits.

The population of the magnons with $k=0$ $[\equiv n(0)]$ is determined by the balance between the excitation and the relaxation,

$$\frac{dn(0)}{dt}=W_{\rm ex}-\frac{n(0)}{T_s}, \tag{8}$$

where $W_{\rm ex}$ is the transition probability of $|00\rangle\rightarrow|1-1\rangle$ per unit time by the microwave irradiation and T_s is the lifetime of the triplet state. At the steady state, $dn(0)/dt=0$, so that $n(0)=W_{\rm ex}T_s$. As the microwave irradiation is shut off, the *spins* start to relax to the ground state ($\sigma_z=-1$) with the relaxation time given by T_s.

We finish this section with a few remarks on the nature of the excited states. One is about the lifetime of the excited states (T_s); it can be rather long due to the primary forbiddance for the electric dipolar transitions. Although the forbiddance itself is usually lifted by some additional interactions such as the Dzyaloshinsky-Moriya interaction [25,26], the primary forbiddance may cause rather long T_s and narrower transition lines. These features are favorable for the selective excitation. The other is about the wave number of the excited magnons; in the present excitation, only the transition to the $k=0$ mode is allowed and that to the staggered mode ($k=a/\pi$) is forbidden. This fact is favorable for the long-range internuclear coupling. Note that the magnons excited by the microwave are in the nonequilibrium states far from the thermal equilibrium, where $k=a/\pi$ magnons are primarily excited.

IV. INTERNUCLEAR COUPLINGS MEDIATED BY $k=0$ MAGNONS

We next look into the details of the longitudinal component of the SN interaction caused by the $k=0$ magnon packet. For simplicity, we assume the following on-site anisotropic hyperfine Hamiltonian in the ith site,

$$H_{hf}=\{A_\parallel s_{i1}^z I_i^z+\tfrac{1}{2}A_\perp(s_{i1}^+I_i^-+s_{i1}^-I_i^+)\}, \tag{9}$$

which can be rewritten using the *spin* introduced in Eq. (6) as

$$H_{hf}=\frac{1}{4}A_\parallel(I_i^z\sigma_i^z-I_i^z)+\frac{1}{2\sqrt{2}}A_\perp(\sigma_i^+I_i^-+\sigma_i^-I_i^+). \tag{10}$$

Hence, besides the term $-\frac{1}{4}A_\parallel I_i^z$, which can be incorporated into the Zeeman term in the nuclear Hamiltonian, the nuclear interaction with the spin σ can be expressed by the anisotropic hyperfine interaction. The first term creates the shifts at the nuclear sites corresponding to H_{tr} and the SN interactions, and the other terms give rise to the spin-lattice relaxation (T_1) [33–35].

Since the transverse component of the SN interaction due to $\sigma^\pm$ vanishes in the field gradient, we restrict ourselves to the longitudinal component. The longitudinal component of the SN interaction is given by [36]

$$H_{SN}=W_{ij}I_i^zI_j^z, \tag{11}$$

where,

$$W_{ij}=\left(\frac{\gamma_n A_\parallel}{N}\right)^2\sum_{k,k',k\neq k'}\frac{n_k-n_{k'}}{\epsilon_{k'}-\epsilon_k}\cos\{(k-k')r_{ij}\}. \tag{12}$$

Here, n_k and ϵ_k are, respectively, the population and the energy of the magnon with the wave number k, and r_{ij} is the

distance between the two nuclei of interest. In the equilibrium states, n_k is given by the Bose function for the given temperature.

Actually, Eq. (11) is a special case of the general formulas for the indirect spin-spin interaction [37,38]

$$H_{ind}=\Phi(r_{ij})I_i^z I_j^z, \tag{13}$$

with the range function

$$\Phi(r_{ij})=\gamma_n^2 A_\parallel^2 \sum_q \chi(q)\exp(iqr_{ij}). \tag{14}$$

Here, $\chi(q)$ is the zero-energy component of the generalized susceptibility and $q=k-k'$. For the pair of nuclei far apart, the most important interaction comes from the uniform part of the susceptibility, i.e., $q\sim 0$. In the present case, the electronic state is not in the equilibrium state, so that $\chi(q)$ is different from that in the thermal equilibrium. Note, in particular, that the magnons with $|k|\gg 0$ such as $k=\pi/a$ are not excited here.

The range to which this interaction reaches depends on the range function $\Phi(r_{ij})$, which is determined by the functional form of $\chi(q)$ as a function of q. For the *transverse* SN interactions in three dimensions (3D), $\Phi(r_{ij})$ can be calculated only from the magnon dispersions. Assuming a parabolic dispersion, it has the form $\sim a/r\exp(-r/3a)$, which is rather short ranged [16]. Unlike this case, however, $\Phi(r_{ij})$ is expected to reach a rather long distance in the present case, i.e., the longitudinal SN interaction in 1D, because of the following reasons; (1) in the longitudinal component, both the number of excited magnons n_k and the magnon dispersions are responsible for $\chi(q)$ and thus $\Phi(r_{ij})$ [see Eq. (12)], (2) the system is not in the equilibrium state and $n_{k=\pi/a}\sim 0$ in the present case, and (3) the $\chi(q)$ structure in 1D is qualitatively different from that in 3D. Since $\chi(q)$ is enhanced at $q\sim 0$ in the present case, a rather long-range interaction is expected.

Here, we estimate the range function for the case of Fig. 4 using Eq. (12). Suppose the magnon dispersion of the spin ladder in the form [39] $\epsilon(k_n)=C+J_\perp(j_1-j_1^3/4)\cos(k_n)+\cdots$, where $k_n=n\pi/N$, $j_1=J_\parallel/J_\perp$, and C is the part independent of k_n. Since $n(k)=0$ for $k\neq 0$, W_{ij} can be calculated as

$$W_{ij}=\frac{2\gamma_n^2A^2\{n(0)/N\}}{J_\perp\left(j_1-\frac{1}{4}j_1^3\right)}\frac{1}{N}\sum_{n=1}^{N}\frac{\cos(k_n r_{ij})}{\cos(k_n)-1}\equiv XF(r_{ij}/a,N). \tag{15}$$

where $X\equiv 2\gamma_n^2A^2\{n(0)/N\}/J_\perp(j_1-j_1^3/4)$. Assuming $A=100$ kOe/μ_B, $\gamma_n/(2\pi)=4.3$ MHz/kOe (in the case of ^1H), $J_\perp=50$ K, $j_1=0.2$ and $n(0)/N=0.01$, one obtains $X=17$ kHz. On the other hand, the range function $F(r_{ij}/a,N)$ in Eq. (15) can be calculated as shown in Fig. 5, which is in the range between -30 and 20. In comparison with the nuclear dipole couplings in solids (~ 10 kHz) [11,12] and the J couplings in solution NMR QCs (10^1–10^3 Hz) [5,6], one finds that the SN coupling can be strong enough to serve as quantum gates. It should be noted that the strength of the coupling W_{ij} can be controlled by the microwave intensity via $n(0)$; it is determined by the balance between excitation and relaxation, and in the steady state, $n(0)=W_{ex}T_s$.

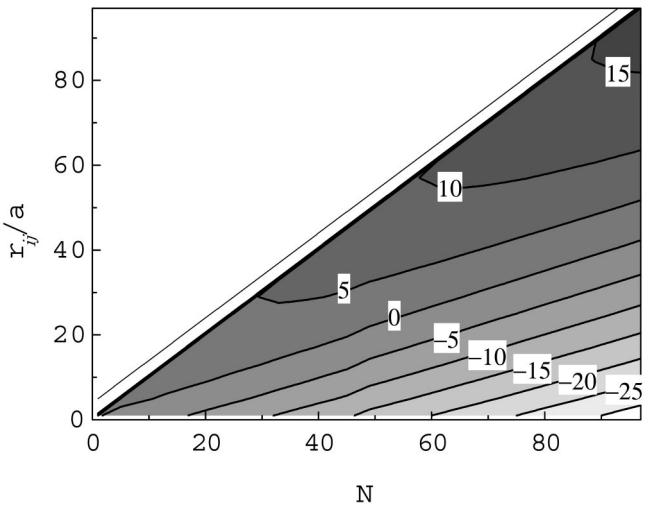

FIG. 5. Contour plot of the range function $F(r_{ij}/a,N)$ in Eq. (15), where r_{ij} is the distance between the C and T qubits and N is the number of lattice points included in the triplet packet.

V. QC INTEGRATION AND NUCLEAR ALIGNMENT

So far, we have described the model for a *single* QC. Unfortunately, the sensitivities of the current NMR detection techniques, even with the state-of-the-art ones, are far below the level required for the single QC detection. In the case of ^{13}C, for example, the minimum number of nuclei that can be observed by these techniques is estimated to be about 10^{16} [40]. This means that the integration of many equivalent QCs is inevitable to obtain the results of computations. The integration of QCs, however, is traded off against the decoherence by the nuclear dipole couplings between QCs; in order for a spin chain to work as an independent QC, the chain should be isolated from the others by reserving spaces between chains to the extent that the decoherence is reasonably small. The reserved spaces, on the other hand, cause lower nuclear density and makes the detection of the signal more difficult. This is a dilemma that always exists in the implementation of the solid-state NMR QCs.

Suppose that many equivalent 1D QCs (^{13}C qubit) are embedded in a bulk material with their axes parallel to the field gradient (see Fig. 7). Here, one qubit is represented by many magnetically equivalent ^{13} C nuclei on a plane perpendicular to the field gradient. For the given interchain distance of r, the coherence time caused by the neighboring nucleus on the same plane is given by $T_{2d}\sim 2r^3/3(^{13}\gamma_n)^2\hbar$, while the area density of the equivalent ^{13} C nuclei on the plane is given by $n=r^{-2}$. The r dependences of T_{2d} and n are shown in Fig. 6. Provided the acceptable coherence time $T_{2d}\sim 10$ s, the required interchain distance r is about 10 nm, which corresponds to the area density $n\sim 10^{12}$ cm^{-2}. Hence, for the typical sample dimension of 1 cm$\times$1 cm, the total number of nuclei N is about 10^{12}. This number of nuclei could be detected by usual NMR detection methods (N

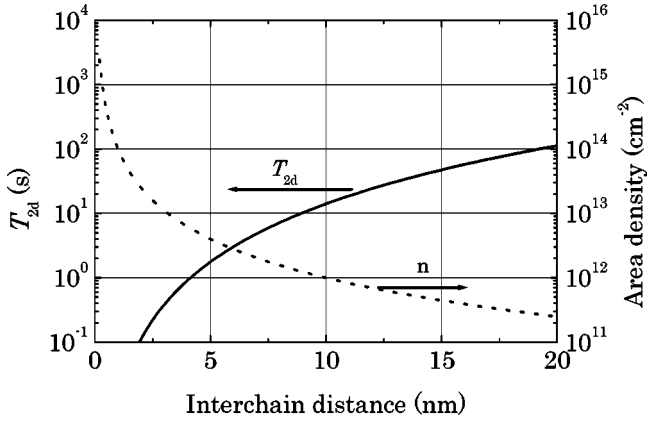

FIG. 6. Interchain distance r dependences of the area density n of ^{13}C and the coherence time T_{2d} caused by the dipole couplings between chains.

$\sim 10^{16}$) if the nuclei are aligned by the dynamical nuclear polarization techniques [41], which could enhance the NMR signal by up to 10^5 [42].

The nuclear alignment is indispensable also for qubit initialization, especially for the large number of qubits ($q \gg 10$); the number of QCs which happen to be in the pure state in the thermal equilibrium is proportional to $(\hbar\omega_n/2k_BT)q/2^q$, which becomes smaller and smaller as increasing q. The nuclear alignment can increase the number of nuclei in the pure state, and the initialization can be achieved with this partially aligned nuclei, using the pseudo-pure state technique [8–10] and the algorithmic cooling method [43,44].

Here, we propose a possible configuration of an optical pumping qubit initializer, which partially aligns the qubits in the spin chains using semiconductors by the optical pumping and the polarization transfer techniques [45]. The scheme enables us to separate the materials responsible for the initialization (semiconductors) and computation (spin chains), so that one can optimize the latter independently of the former. The schematic illustration is shown in Fig. 7. Quantum spin chains and semiconductors (e.g., Si, GaAs) are multilayered and attached to a flat board micromagnet, which produces a magnetic-field gradient [18].

The electrons in the semiconducting layers are polarized by circularly polarized near-infrared laser lights with the energy corresponding to the semiconducting gap [46,47], and the polarization is transferred to the nuclear spins in the spin chains at the interfaces by the cross-polarization/coherent transfer techniques [48] or hyperfine couplings [49–51]. The nuclear polarizations at the interfaces further diffuse into the inner part of the spin chain layer through the nuclear dipole couplings between isospins on the planes of equivalent qubits. On completion of the initialization, the laser is shut off, and the semiconducting layers return to the silent environment. Once the computation starts, the nuclear dipole couplings on the plane of equivalent qubits are decoupled using a high power decoupler.

VI. PRACTICAL IMPLEMENTATION

In this final section, we discuss practical implementations of the scheme. The most critical issue is to find a suitable

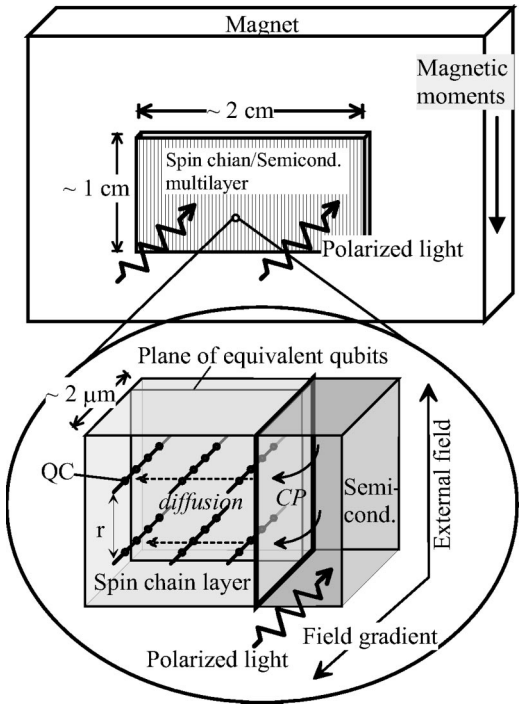

FIG. 7. A possible configuration of the optical pumping qubit initializer, which has a multilayer structure of the quantum spin chains and semiconductors (SC) attached to a flat board magnet. The enlargement shows the interface between the spin chain and SC layers. In the spin chain layer, 1D QCs (balls denote qubits) are aligned apart from each other by several lattice spacings (r). The electrons in the SC layers are optically pumped by laser lights delivered from the front. The polarizations thus created in the SC layers are transferred to the inner part of the spin chain layers both through a cross polarization (CP) via the heterospin couplings and a spin diffusion via the isospin couplings. Typical dimensions of the sample are also shown.

quantum spin chain system with a singlet ground state, containing more than two stable isotopes for one element, one of which has $I=1/2$. Moreover, the periodical placements of the 1/2 nuclear spins may require some appropriate techniques.

One possible candidate is organic materials. Examples include (1) spin-Peierls systems such as $(TTF)AuS_4C_4(CF_3)_4$ (TTF=tetrathiafulvalene), $MEM(TCNQ)_2$ (MEM=N-methyl-N-ethylmurpholinum), $Cu_2(C_5H_{12}N_2)_2Cl_4$, (2) Haldane systems such as $Ni(C_2H_8N_2)_2NO_2ClO_4$, $Ni(C_3H_{10}N_2)NO_2ClO_4$, and (3) spin-ladder systems such as (BEDT-TTF)$Zn(SCN)_3$ (BEDT-TTF = bis(ethylene-dithio)-tetrathiafulvalene). The merits of these materials are that ^{1}H($I=1/2$) and ^{13}C ($I=1/2$) are available as qubits, and that their large unit cells allow us to reserve large spacial distances between qubits. Moreover, one can utilize the selective isotope replacement technique known as ''isotope labeling,'' such as the ^{2}D substitution for a hydrogen site [52] or ^{13}C for a carbon site [53]. This method, together with the epitaxial growth (molecular-beam epitaxy, MBE) [54] and/or the Langmuir-Blodgett (LB) methods, may allow us to arrange qubit nuclei periodically along a spin chain as follows: one prepares two sets of the same kind of molecule, in one of

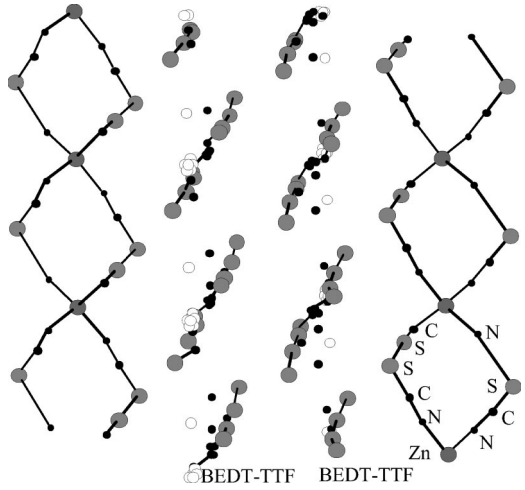

FIG. 8. Crystal structure of (BEDT-TTF)$Zn(SCN)_3$ projected onto the long molecular axis. The double chains of the ET molecules form a spin ladder.

which isotope labeling is performed [e.g., ^{13}C is substituted in a BEDT-TTF molecule of (BEDT-TTF)$Zn(SCN)_3$]. These two sets of molecules are piled up epitaxially in order using either the MBE or the LB method, so that the ^{1}H's or ^{13}C's are lined up in one direction periodically.

In order to avoid unnecessary nuclear couplings, it is preferable that nuclei other than qubits have no spins ($I=0$). In this sense, it is fortunate that major abundant isotopes in organic materials such as ^{12}C and ^{16}O have no spins. In addition, one can use a high power decoupler and/or decoupling sequences between unlike spins to remove the effects of the nonzero-spin nuclei such as ^{2}D and ^{14}N. The only disadvantage of the organic materials is that the typical values of the hyperfine couplings for ^{1}H and ^{13}C are very small, as shown below.

In the following, we discuss the case of (BEDT-TTF)$Zn(SCN)_3$ as an example, which has a two-leg ladder consisting of BEDT-TTF (ET) molecules as shown in Fig. 8 [55,56]. Qubits are ^{13}C ($\gamma_n/2\pi=1.07$ MHz/kOe) substituted in the ET molecules. The ^{13}C labeling of the specific site of the ET molecule has been established [53]. We suppose that the ET molecules with and without ^{13}C nuclei can be piled up in order along one of the two legs by the epitaxial growth technique, although this has not yet been confirmed.

The switching time for the SN (controlled-NOT) gate ($1/2W_{ij}$) is estimated as follows. The exchange interactions in this material were reported to be $J_\perp=996$ K and $J_\parallel=86$ K [55]. The magnon dispersion deduced from the T dependence of the susceptibility is given as $\epsilon(k)=\Delta-4\epsilon_0\cos(k)+\cdots$ with $\Delta/k_B=340$ K and $\epsilon_0/k_B=62$ K, while the hyperfine coupling constant in the ^{13}C site in the ET molecule ($A_\parallel$) is about 2 kOe/μ_B [53]. Provided that $n(0)/N=0.05$ and $F(r_{ij}/a,N)=20$, W_{ij} in Eq. (15) is calculated to be about 12 Hz ($1/2W_{ij}\sim 40$ ms). Although W_{ij} is rather small due to the small $A_\parallel$, it is still of the same order as the J couplings in solution QCs.

The number of equivalent nuclei necessary for each qubit depends on the efficiencies of the optical pumping and the polarization transfer. Tycko estimated the number of equivalent nuclei required to observe ^{13}C nuclei in an organic material on a semiconducting substrate [45]. Assuming 10% of the polarization in the substrate and 5% of the transfer efficiency, they estimated that the signals from $N=10^{14}$ equivalent nuclei can be observed with the signal-to-noise ratio of unity at 9 T and 300 K with 16 scans, which corresponds to $N=10^{12}$–10^{13} at 4 K in a single-shot measurement. The number of available nuclei for each qubit, $N\sim 10^{12}$ (see Sec. V), falls within this range.

The main sources of decoherence in this system are twofold; nuclear dipole couplings and inhomogeneity of the magnetic field in the plane of equivalent qubits. The contribution of the dipolar field from nonqubit nuclei can be zero using zero-spin isotopes (^{12}C, ^{64}Zn, ^{32}S, etc.) and/or the decouplers (^{14}N and ^{1}H). The residual dipolar couplings are those between ^{13}C-^{13}C isospins, which can be of the order of 10 s as estimated in the preceding section. On the other hand, the effect of the inhomogeneous field depends on the dimension of the sample. According to the simulation for a magnetic field produced by a Dy micromagnet [18], it is possible to generate a field homogeneity of 10 ppm over the dimension of 2 cm$\times$1 μm in the plane perpendicular to the magnetic-field gradient, which is as small as that in a commercial high-resolution NMR magnet. Moreover, the dephasing effect due to such inhomogeneity can be eliminated by appropriate refocusing pulses.

ACKNOWLEDGMENTS

We are indebted to G. Kido and M. Kitagawa for helpful advice. Technical support by S. Eguchi is also acknowledged. This work was partially supported by the Industrial Technology Research Grant Program in 2002 from the New Energy and Industrial Technology Development Organization (NEDO) of Japan.

[1] D. Deutsch, Proc. R. Soc. London, Ser. A **400**, 97 (1985).
[2] P.W. Shor, SIAM J. Comput. **26**, 1417 (1997).
[3] L.K. Grover, Phys. Rev. Lett. **80**, 4329 (1998).
[4] D. DiVincenzo, Phys. Rev. A **51**, 1015 (1995).
[5] I.L. Chuang, N. Gershenfeld, and M. Kubinec, Phys. Rev. Lett. **80**, 3408 (1998).
[6] J.A. Jones and M. Mosca, J. Chem. Phys. **109**, 1648 (1998).
[7] L.M.K. Vandersypen, M. Steffen, G. Breyta, C.S. Yannoni, M.H. Sherwood, and I.L. Chuang, Nature (London) **414**, 883 (2001).
[8] N.A. Gershenfeld and I.L. Chuang, Science **275**, 350 (1997).
[9] D.G. Cory, A.F. Fahmy, and T.F. Havel, Proc. Natl. Acad. Sci. U.S.A. **94**, 1634 (1997).

[10] E. Knill, I.L. Chuang, and R. Laflamme, Phys. Rev. A **57**, 3348 (1998).
[11] F. Yamaguchi and Y. Yamamoto, Appl. Phys. A: Mater. Sci. Process. **68**, 1 (1999).
[12] T.D. Ladd, J.R. Goldman, F. Yamaguchi, and Y. Yamamoto, Appl. Phys. A: Mater. Sci. Process. **71**, 27 (2000).
[13] A. Goto, T. Shimizu, R. Miyabe, K. Hashi, H. Kitazawa, G. Kido, K. Shimamura, and T. Fukuda, Appl. Phys. A: Mater. Sci. Process. **74**, 73 (2002).
[14] M.A. Ruderman and C. Kittel, Phys. Rev. **96**, 99 (1954).
[15] H. Suhl, Phys. Rev. **109**, 606 (1958).
[16] T. Nakamura, Prog. Theor. Phys. **20**, 542 (1958).
[17] A. Goto, T. Shimizu, and K. Hashi, J. Phys. Soc. Jpn. **71**, 2125 (2002).
[18] J.R. Goldman, T.D. Ladd, F. Yamaguchi, and Y. Yamamoto, Appl. Phys. A: Mater. Sci. Process. **71**, 11 (2000).
[19] M. Itoh, M. Sugahara, T. Yamauchi, and Y. Ueda, Phys. Rev. B **54**, R9631 (1996).
[20] A.W. Sandvik, E. Dagotto, and D.J. Scalapino, Phys. Rev. B **53**, R2934 (1996).
[21] J. Kishine, J. Phys. Soc. Jpn. **66**, 1229 (1997).
[22] S.R. White, R.M. Noack, and D.J. Scalapino, Phys. Rev. Lett. **73**, 886 (1994).
[23] A. Barenco, C.H. Bennett, R. Cleve, D.P. DiVincenzo, N. Margolus, P. Shor, T. Sleator, J.A. Smolin, and H. Weinfurter, Phys. Rev. A **52**, 3457 (1995).
[24] D. Collins, K.W. Kim, W.C. Holton, H. Sierzputowska-Gracz, and E.O. Stejskal, Phys. Rev. A **62**, 22304 (2000).
[25] T.M. Brill, J.P. Boucher, J. Voiron, G. Dhalenne, A. Revcolevschi, and J.P. Renard, Phys. Rev. Lett. **73**, 1545 (1994).
[26] W. Lu, J. Tuchendler, M. von Ortenberg, and J.P. Renard, Phys. Rev. Lett. **67**, 3716 (1991).
[27] M. Tachiki and T. Yamada, J. Phys. Soc. Jpn. **28**, 1413 (1970).
[28] D. Augier and D. Poilblanc, Eur. Phys. J. B **1**, 19 (1998).
[29] G.S. Uhrig and H.J. Schulz, Phys. Rev. B **54**, R9624 (1996).
[30] A.W. Garrett, S.E. Nagler, D.A. Tennant, B.C. Sales, and T. Barnes, Phys. Rev. Lett. **79**, 745 (1997).
[31] W. Yu and S. Haas, Phys. Rev. B **62**, 344 (2000).
[32] B. Grenier, L.P. Regnault, J.E. Lorenzo, J.P. Boucher, A. Hiess, G. Dhalenne, and A. Revcolevschi, Phys. Rev. B **62**, 12 206 (2000).
[33] D. Beeman and P. Pincus, Phys. Rev. **166**, 359 (1968).
[34] M.W. Pieper, J. Kotzler, and K. Nehrke, Phys. Rev. B **47**, 11 962 (1993).
[35] D.A. Ivanov and P.A. Lee, Phys. Rev. B **59**, 4803 (1999).
[36] V. Zevin and N. Kaplan, Phys. Rev. B **12**, 4604 (1975).
[37] C.H. Pennington and C.P. Slichter, Phys. Rev. Lett. **66**, 381 (1991).
[38] Y. Itoh, H. Yasuoka, T. Machi, Y. Fujiwara, K. Tai, I. Tomeno, N. Koshizuka, and S. Tanaka, J. Phys. Soc. Jpn. **61**, 1287 (1992).
[39] M. Muller and H.-J. Mikeska, J. Phys.: Condens. Matter **12**, 7633 (2000).
[40] Y.S. Greenberg, Rev. Mod. Phys. **70**, 175 (1998).
[41] R. R. Ernst, G. Bodenhausen, and A. Wokaun, *Principles of Nuclear Magnetic Resonance in One and Two Dimensions*, International Series of Monographs on Chemistry Vol. 14 (Oxford University Press, Oxford, 1987).
[42] M. Iinuma, I. Shaké, R. Takizawa, M. Daigo, H.M. Shimizu, Y. Takahashi, A. Masaike, and T. Yabusaki, Phys. Lett. A **208**, 251 (1995).
[43] L. J. Schulman and U. V. Vazirani, Proceedings of the 31st ACM Symposium on Theory of Computing 1999 (unpublished), p. 322.
[44] T.D. Ladd, J.R. Goldman, F. Yamaguchi, Y. Yamamoto, E. Abe, and K.M. Itoh, Phys. Rev. Lett. **89**, 17 901 (2002).
[45] R. Tycko, Solid State Nucl. Magn. Reson. **11**, 1 (1998).
[46] G. Lampel, Phys. Rev. Lett. **20**, 491 (1968).
[47] *Optical Orientation*, edited by F. Meier and B. P. Zakharchenya, Modern Problems in Condensed Matter Science, Vol. 8 (North-Holland, Amsterdam, 1984).
[48] C. P. Slichter, *Principles of Magnetic Resonance*, Springer Series of Solid State Sciences, Vol. 1 (Springer-Verlag, Berlin, 1990).
[49] C.A. Michal and R. Tycko, Phys. Rev. Lett. **81**, 3988 (1998).
[50] C.A. Michal and R. Tycko, Phys. Rev. B **60**, 8672 (1999).
[51] W. Farah, M. Dyakonov, D. Scalbert, and W. Knap, Phys. Rev. B **57**, 4713 (1998).
[52] S. Aonuma, H. Sawa, Y. Okano, R. Kato, and H. Kobayashi, Synth. Met. **58**, 29 (1993).
[53] A. Kawamoto, K. Miyagawa, Y. Nakazawa, and K. Kanoda, Phys. Rev. Lett. **74**, 3455 (1995).
[54] T.J. Schuerlein, A. Schmidt, P.A. Lee, K.W. Nebesny, and N.R. Armstrong, Jpn. J. Appl. Phys., Part 1 **34**, 3837 (1995).
[55] T. Komatsu, N. Kojima, and G. Saito, Synth. Met. **103**, 1923 (1999).
[56] H. Mori, S. Tanaka, T. Mori, and Y. Maruyama, Bull. Chem. Soc. Jpn. **68**, 1136 (1995).